소형공작기계의 기하학적 오차 평가를 위한 다자유도 측정시스템

권성환*(경북대 대학원), 리우위(경북대 대학원), 양승한(경북대)

A Multi-Degree of Freedom Measurement System for Determining Geometric Errors in Miniaturized Machine Tool

S. H. Kweon (Graduate School, Mechanical. Eng. Dept. KNU), Y. Liu (Graduate School, Mechanical Eng. Dept., KNU), S. H. Yang (Mechanical Eng. Dept., KNU)

ABSTRACT

소형화된 기계가공시스템은 사용재료의 다양화와 에너지 및 공간의 감소와 같은 장점을 가지고 작고 정밀한 부품을 가공할 수 있는 시스템으로 주목 받고 있다. 이러한 시스템이 비록 그 크기가 일반적인 가공시스템에 비해 작지만 정렬 및 조립공정, 기계요소의 불완정성에 의한 기하학적 오차는 여전히 존재한다. 기하학적 오차 평가는 기계시스템의 정밀도를 효과적으로 적은 비용으로 향상시킬 수 있는 오차보정기술을 적용할 수 있는 토대가 된다. 일반적으로, 3 축의 직선축으로 이루어진 공작기계는 21 개의 오차요소를 가진다. 레이져간섭계는 이러한 오차요소를 평가하는데 널리 사용되고 있지만 광학계를 정렬하고 설치하는 데 많은 어려움이 있으며 한번의 설치로 한 개의 오차요소만이 측정 가능하다. 또한, 소형공작기계의 경우, 그 크기로 인해 기존의 레이져 간섭계를 직접적으로 적용할 수 없다. 따라서, 본 연구에서는 소형공작기계를 포함한 소형가공시스템의 기하학적 오차 평가를 위한 새로운 다자유도 측정시스템을 제안하였다. 5 개의 정전용량변위 센서를 사용하는 이 시스템을 통해 한 축의 움직임에 따른 5 개의 오차요소를 동시에 측정 가능 하다. 균질변환행렬을 이용한 측정알고리듬을 구성하고 이를 모의시험을 통해 평가하였다. 수학적 모델링을 통해 각 센서의 출력값을 유도하고 이를 이용하여 각 오차요소를 계산하기 위한 식을 유도하였다. 여기서, 단순화된 식을 적용한 경우, 임의의 오차에 대한 측정 알고리듬의 정확도를 평가하였다. 또한, 측정 시스템의 설치시 발생하는 셋업오차에 대한 측정 알고리듬의 민감도 분석을 행하였다. 제안하는 측정 시스템은 구조가 간단하고 고가의 부가장비가 필요치 않다. 또한, 적은 비용으로 구성할 수 있으며 높은 측정 정밀도를 가지고 소형가공시스템에 필요한 오차 평가를 행할 수 있다.

Key Words : Geometric error(기하학적 오차), Homogeneous transformation matrix (균질변환행렬), Multi-DOF measurement system(다자유도측정시스템), Miniaturized Machine Tool(소형공작기계), Capacitance sensor

1. Introduction

Miniature components are increasingly needed for a wide range of applications in the fields of biotechnology, aerospace, semi-conductor industry, electronics, medical robotics, and optics. Part materials include stainless steel, brass, aluminum, and even glass. To manufacture such small parts, the Miniaturized Machine Tool (mMT) is presented as an alternative to combine the advantages of the existing methods, i.e. LIGA, MEMS, and ultra-precision conventional machining method [1]. In the research of miniature machine tools, accuracy enhancement of machine tools is still one of the most critical concerns, which is mainly affected by geometric errors, thermal errors and cutting-force induced errors. In these error sources, geometric error is a major contributor to the workpiece errors.

Error compensation technique has been developed as a cost-effective method to achieve further improvement of the machine accuracy since 1970s. In the error compensation techniques, the crucial task is how to gather necessary information about the interested errors.

Conventional measurement technique and methodology range from the use of laser interferometers, electronic levels, mechanical squares, straight edges, and other devices [2].

For a three-axis machine tool, however, the complete measurement of 21 geometric error components by the conventional means is very time consuming. Zhang [3] developed a displacement method to assess the 21 geometric errors through linear displacement measurement along 22 lines in the working volume. Later, a Multi-Degree-of-Freedom Measurement System (MDFM system) for identifying five geometric error components simultaneously was developed by Ni [4]. To measure up to six geometric error components at a time, Fan [5] reported a six-degree-of-freedom measurement system (6DMS) and in the calibration of this system it has shown good results compatible with the HP 5528A interferometer.

But direct application of conventional devices to the measurement of geometric errors on the mMT is not feasible due to the order of magnitude of the reduction in working volume of miniaturized machine tool, whose whole dimensions are only 350 mm×250 mm ×400 mm in our case. To tackle such problems, a size-compact, low-cost and enough accurate multi-degree-of-freedom measurement system is needed for the study of mMT.

This paper begins with a brief introduction about the multi-degree-of-freedom measurement system. Using the Homogeneous Transformation Matrix (HTM), an exact mathematical model is extracted to describe the output of every probe. Based on this exact model, a simple algorithm is developed to obtain the five error components. Simulation and error analysis are also presented to show the effects of different factors contributing to the accuracy of these methods. The proposed algorithms are evaluated and the results are presented.

2. System Configuration

The prototype of our vertical miniaturized machine tool is shown in Fig.1. The stepping motor is adopted as the driver with the step size of 0.36 °. Non-contact optical linear encoder (Renishaw Inc.) is chosen as the feedback sensor, whose high accuracy, repeatability and linearity can keep the linear displacement error within 50 nanometers. This value of linear displacement error is so small compared with other error components that it could be though as zero. The spindle holder is fixed on the Z-carriage. Z-carriage moves vertically along the vertical column with a prismatic joint. The column is bolted on the bed. The Y-carriage is stacked and moves horizontally on the X-carriage with a prismatic joint, and the X-carriage is on the bed with a prismatic joint, too.

Fig. 2 shows the schematic diagram of the proposed multi-DOF measurement system. It consists of two parts--the fixture, which is used to fix five capacitance probes (A, B, C, D and E), and the target as the measured surface. The fixture is installed on the position of tool holder and the target part is fixed on the motion stage. Five probes are divided into two units: top unit composed of three probes can measure vertical straightness error, pitch error and roll error; and the side unit with two probes can measure the horizontal straightness error and yaw error.

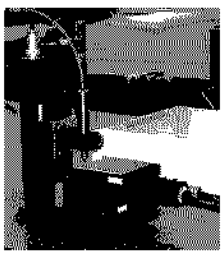

Fig.1 The system prototype of vertical mMT

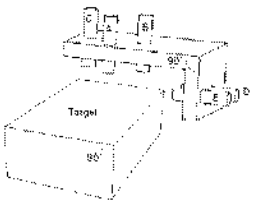

Fig.2 Schematic of multi-DOF measurement system

3. Exact Mathematical Model

As shown in Fig.3, O_M- X_M Y_M Z_M is the metrological reference coordinate frame, and O1-X1Y1Z1 is the carriage coordinate frame. When we measure geometric errors in the X and Y direction, the Z-axis is adjusted and locked. When the motion table moves in X-axis, there are six geometric error components existing (Fig.3): linear displacement error $\delta_{xx}(d)$, horizontal straightness error $\delta_{yx}(d)$, vertical straightness error $\delta_{zx}(d)$, roll error $\varepsilon_{xx}(d)$, pitch error $\varepsilon_{yx}(d)$ and yaw error $\varepsilon_{zx}(d)$. The letter "d" in bracket, given here specially, implicates the commanded linear displacement in intended motion direction. For convenience, we simply express the six errors as δ_{xx}, δ_{yx}, δ_{zx}, ε_{xx}, ε_{yx} and ε_{zx}.

After a linear displacement d, O1-X1Y1Z1 has transformed to O'1-X'1Y'1Z'1(Fig.4) because of the six

geometric error components.

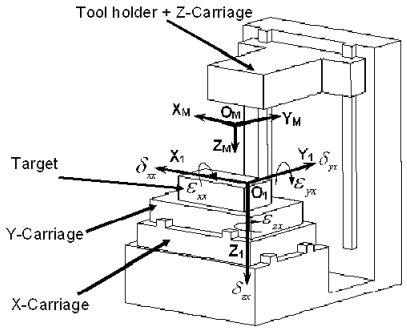

Fig.3 Schematic of six geometric error motions

With the assumption of rigid body and small rotational errors, the measured pointP1 (x_{p1}, y_{p1}, z_{p1}) corresponds to P0 (x_{p0}, y_{p0}, z_{p0}) before the linear displacement d. The relation between P0 and P1 can be represented by the well-known HTM [6]:

$$T = \begin{pmatrix} 1 & -\varepsilon_{zx} & \varepsilon_{yx} & d+\delta_{xx} \\ \varepsilon_{zx} & 1 & -\varepsilon_{xx} & \delta_{yx} \\ \varepsilon_{yx} & \varepsilon_{xx} & 1 & \delta_{zx} \\ 0 & 0 & 0 & 1 \end{pmatrix}$$

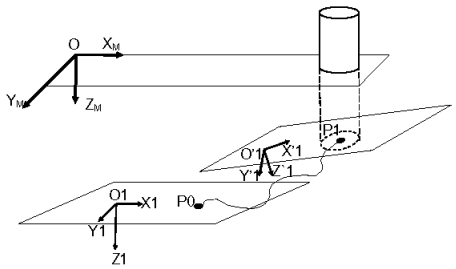

Fig.4 Schematic of the measurement principle

If (x_{p1}, y_{p1}) of P1 is known, (x_{p0}, y_{p0}, z_{p0}) of P0 can be obtained by:

$$\begin{pmatrix} x_{p0} & y_{p0} & z_{p0} & 1 \end{pmatrix}^T = T^{-1} \begin{pmatrix} x_{p1} & y_{p1} & z_{p1} & 1 \end{pmatrix}^T \text{--(1)}$$

Then, it is easy to derive from Equation (1):

$$z_{p0} = \frac{x_{p1}(\varepsilon_{yx}+\varepsilon_{xx}\varepsilon_{zx}) + y_{p1}(-\varepsilon_{xx}+\varepsilon_{yx}\varepsilon_{zx}) + z_{p1}(1+\varepsilon_{zx}^2)}{1+\varepsilon_{xx}^2+\varepsilon_{yx}^2+\varepsilon_{zx}^2} + \frac{(-\delta_{zx}+\delta_{yx}\varepsilon_{xx}-\delta_{yx}\varepsilon_{yx}\varepsilon_{zx}-\delta_{zx}\varepsilon_{zx}^2-\delta_{xx}\varepsilon_{yx}-\delta_{xx}\varepsilon_{xx}\varepsilon_{zx}) + (-d\varepsilon_{yx}-d\varepsilon_{xx}\varepsilon_{zx})}{1+\varepsilon_{xx}^2+\varepsilon_{yx}^2+\varepsilon_{zx}^2}$$

There is such case existing that $z_{p1} = z_{p0} + \Delta z$ in which Δz characterizes the relative output of probe and z_{p0} is zero since the point is chosen on the target surface. Then,

$$\Delta z = z_{p1} = \frac{1}{1+\varepsilon_{zx}^2}(\varepsilon_{xx}(y_{p1}-\delta_{yx}+(d-x_{p1}+\delta_{xx})\varepsilon_{zx}) + \varepsilon_{yx}(d-x_{p1}+\delta_{xx}+(-y_{p1}+\delta_{yx})\varepsilon_{zx})+\delta_{zx}(1+\varepsilon_{zx}^2)) \text{--(2)}$$

Equation (2) describes the output of probe by using related geometric errors.

Fig. 5(a) shows the arrangement of the top probes. Substituting the coordinate vector of each probe into Equation (2), the Exact Mathematical Model, which describes the changes in output of every probe incorporated with these geometric error components:

$$\Delta z_A = \frac{1}{1+\varepsilon_{zx}^2}(\varepsilon_{xx}(-\delta_{yx}+(d-\ell+\delta_{xx})\varepsilon_{zx}) + \varepsilon_{yx}(d-\ell+\delta_{xx}+\delta_{yx}\varepsilon_{zx}) + \delta_{zx}(1+\varepsilon_{zx}^2)) \text{-------(3)}$$

$$\Delta z_B = \frac{1}{1+\varepsilon_{zx}^2}(\varepsilon_{xx}(\ell-\delta_{yx}+(d+\delta_{xx})\varepsilon_{zx}) + \varepsilon_{yx}(d+\delta_{xx}+(-\ell+\delta_{yx})\varepsilon_{zx}) + \delta_{zx}(1+\varepsilon_{zx}^2)) \text{-------(4)}$$

$$\Delta z_C = \frac{1}{1+\varepsilon_{zx}^2}(\varepsilon_{xx}(-\ell-\delta_{yx}+(d+\delta_{xx})\varepsilon_{zx}) + \varepsilon_{yx}(d+\delta_{xx}+(\ell+\delta_{yx})\varepsilon_{zx}) + \delta_{zx}(1+\varepsilon_{zx}^2)) \text{-------(5)}$$

For the side-probe unit in Fig. 5(b), the same procedure is used to extract their mathematical model. The ℓ' has no effect on relative outputs of the side probes:

$$\Delta y_D = \frac{1}{1+\varepsilon_{xx}^2}(\varepsilon_{xx}(-\ell''+\delta_{zx}+(d+\delta_{xx})\varepsilon_{yx}) + \delta_{yx}(1+\varepsilon_{zx}^2) - (d+\delta_{xx}+(\ell''-\delta_{zx})\varepsilon_{yx})\varepsilon_{zx}) \text{----------(6)}$$

$$\Delta y_E = \frac{1}{1+\varepsilon_{xx}^2}(\varepsilon_{xx}(-\ell''+\delta_{zx}+(d-\ell+\delta_{xx})\varepsilon_{yx}) + \delta_{yx}(1+\varepsilon_{zx}^2) - (d-\ell+\delta_{xx}+(\ell''-\delta_{zx})\varepsilon_{yx})\varepsilon_{zx}) \text{-------(7)}$$

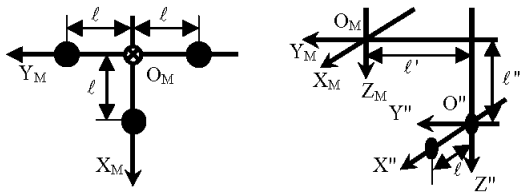

(a) Top probe unit (b) Side probe unit

Fig.5 Position distribution of sensors in 3-D space

4. Algorithm for Geometric Errors

With the aforementioned case that δ_{xx} can be neglected, the five geometric errors can be calculated by the algorithm derived from Equations (3~7) through mathematical elimination methods:

$$\hat{\varepsilon}_{xx} = \frac{\Delta z_B - \Delta z_C}{2\ell} \text{----------(8)}$$

$$\hat{\varepsilon}_{yx} = \frac{\Delta z_A - (\frac{\Delta z_B + \Delta z_C}{2})}{-\ell} \text{------(9)}$$

$$\hat{\delta}_{zx} = \frac{\Delta z_B + \Delta z_C}{2} - d\hat{\varepsilon}_{yx} \text{-------(10)}$$

$$\hat{\varepsilon}_{zx} = \frac{\Delta y_E - \Delta y_D}{\ell}; \text{----------(11)}$$

$$\hat{\delta}_{yx} = \Delta y_D + d\hat{\varepsilon}_{zx} + \ell''\hat{\varepsilon}_{xx} \text{-----(12)}$$

where the "^"represents calculated value. In fact, the squareness errors can also be mathematically obtained through using least square fitting method to deal with the measured data about the straightness errors shown in Fig.6 [7].

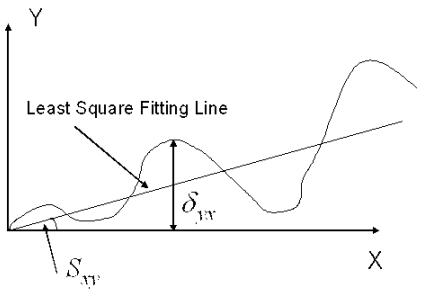

Fig.6 Schematic of least-square method

5. Evaluation of Algorithm

The above algorithm gives us a simplified method to determine the geometric errors. In order to find out these errors, higher than one order of error terms are eliminated so that some accuracy errors are induced in this process. In this paper, the exact mathematical model extracted in previous section is used to study these induced errors. For this purpose, five geometric error components (δ_{yx} , δ_{zx} , ε_{xx} , ε_{yx} and ε_{zx}) are predefined and introduced into Equations (3~7). It is feasible to solve these outputs of all probes Δz_A , Δz_B , Δz_C , Δy_D and Δy_E . Then, the equations (8~12) are applied to obtain $\hat{\delta}_{yx}$, $\hat{\delta}_{zx}$, $\hat{\varepsilon}_{xx}$, $\hat{\varepsilon}_{yx}$ and $\hat{\varepsilon}_{zx}$, which are compared with their predefined values to determine the induced errors. Simulation I (Appendix) shows the induced errors are randomly distributed with the zero mean. For the rotational errors and translational errors, the induced errors are -10^{-6} rad ~ 10^{-6} rad and -0.06 μm ~ 0.06 μm, respectively.

6. Sensitivity Analysis

In this part, the effects of probe-mounting error, resulted from the imperfect machining process of probe position, are investigated first. In common method [8], the authors usually use the partial derivatives of interested variables to study the effect of their variance. Here, another method is used to define the probe-mounting error based on the tolerance which is described by a circle with the nominal position as the center point shown in Fig.7.

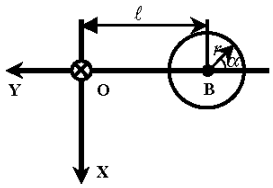

Fig.7 Schematic of probe-mounting error

$$\begin{cases} x_A = \ell + r \times \cos\alpha_A \\ y_A = r \times \sin\alpha_A \end{cases} \quad (13)$$

$$\begin{cases} x_B = r \times \cos\alpha_B \\ y_B = \ell + r \times \sin\alpha_B \end{cases} \quad (14)$$

$$\begin{cases} x_A = r \times \cos\alpha_C \\ y_A = -\ell + r \times \sin\alpha_C \end{cases} \quad (15)$$

In the above Equations (13~15), the polar coordinate forms are used to depict the position variation of every top probe where r (tolerance radius) and angular $\alpha_i (i = A,B,C)$ together decide the possible position on which the probe could be. For the top probe unit, only the coordinates in X-Y plane are considered because the relative changes of output in Z-axis are just our interests, which are not affected by how high this probe is away from the target surface. For the side unit, of course, only the coordinates in X-Z plane are concerned and any deviations in Y-direction do not have effects on the output changes of the side probes.

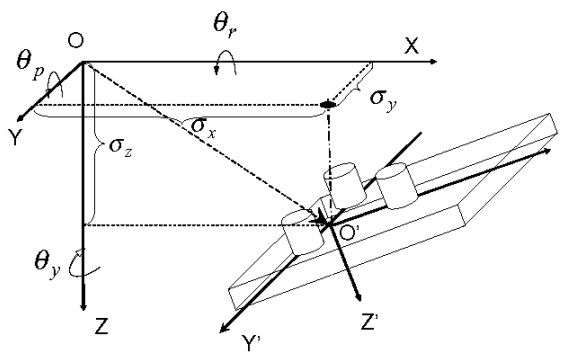

Fig.8 Schematic of installment-dependent error

In the experimental practice, it can not be avoided that installment-dependent errors are induced (illustrated in Fig.8). The installment-dependent errors are divided into two main parts: rotational errors θ_r , θ_p and θ_y errors in fixture installing process; and translational offsets σ_x , σ_y and σ_z . The concept of homogeneous transformation matrix can also be used to deal with them:

$$\begin{pmatrix} x'_{p1} \\ y'_{p1} \\ z'_{p1} \\ 1 \end{pmatrix} = \begin{pmatrix} C\theta_p C\theta_y & -C\theta_p S\theta_y & S\theta_p & \sigma_x \\ (S\theta_r S\theta_p C\theta_y \\ +C\theta_r S\theta_y) & (C\theta_r C\theta_y \\ -S\theta_r S\theta_p S\theta_y) & -S\theta_p S\theta_r & \sigma_y \\ (-C\theta_r S\theta_p C\theta_y \\ +S\theta_r S\theta_y) & (S\theta_r C\theta_y \\ +C\theta_r S\theta_p S\theta_y) & C\theta_r C\theta_p & \sigma_z \\ 0 & 0 & 0 & 1 \end{pmatrix} \begin{pmatrix} x_{p1} \\ y_{p1} \\ z_{p1} \\ 1 \end{pmatrix}$$

where the operators S = sine and C = cosine. Because these three angular errors are very small, the above equation can be written as follow:

$$\begin{pmatrix} x'_{p1} \\ y'_{p1} \\ z'_{p1} \\ 1 \end{pmatrix} = \begin{pmatrix} 1 & -\theta_y & \theta_p & \sigma_x \\ \theta_y & 1 & -\theta_r & \sigma_y \\ -\theta_p & \theta_r & 1 & \sigma_z \\ 0 & 0 & 0 & 1 \end{pmatrix} \begin{pmatrix} x_{p1} \\ y_{p1} \\ z_{p1} \\ 1 \end{pmatrix}$$

Only the position variables in X-Y plane have effects on the output changes of top probe unit and in above transform square matrix any error components related to z coordinate are not considered. Referring to Equation (1), we can get:

$$\begin{pmatrix} x_{p0} \\ y_{p0} \\ z_{p0} \\ 1 \end{pmatrix} = \begin{pmatrix} 1 & -\varepsilon_{zx} & \varepsilon_{yx} & d+\delta_{xx} \\ \varepsilon_{zx} & 1 & -\varepsilon_{xx} & \delta_{yx} \\ \varepsilon_{yx} & \varepsilon_{xx} & 1 & \delta_{zx} \\ 0 & 0 & 0 & 1 \end{pmatrix}^{-1} \begin{pmatrix} 1 & -\theta_y & 0 & \sigma_x \\ \theta_y & 1 & 0 & \sigma_y \\ 0 & 0 & 1 & 0 \\ 0 & 0 & 0 & 1 \end{pmatrix} \begin{pmatrix} x_{p1} \\ y_{p1} \\ z_{p1} \\ 1 \end{pmatrix}$$

Same procedure in Section 3 is used to derive the present output changes of top probe unit:

$$\Delta z' = \frac{(\varepsilon_{zx}(y_{p1} - \delta_{yx} + x_{p1}\theta_y + (d - x_{p1} + y_{p1}\theta_y - \sigma_x)\varepsilon_{zx} + \sigma_y)}{1+\varepsilon_{zx}^2}$$
$$\frac{+\varepsilon_{yx}(d - x_{p1} + y_{p1}\theta_y - \sigma_x + \varepsilon_{zx}(-y_{p1} + \delta_{yx} - x_{p1}\theta_y - \sigma_y)) + \delta_{zx}(1+\varepsilon_{zx}^2))}{1+\varepsilon_{zx}^2}$$

Substituting the position coordinates of every top probe into the above equation, we can get:

$$\Delta z'_A = \frac{1}{1+\varepsilon_{zx}^2}(\varepsilon_{xx}(r\times\sin\alpha_A - \delta_{yx} + (\ell + r\times\cos\alpha_A)\theta_y + (d - (\ell + r\times\cos\alpha_A)$$
$$+(r\times\sin\alpha_A)\theta_y - \sigma_x)\varepsilon_{zx} + \sigma_y) + \varepsilon_{yx}(d - (\ell + r\times\cos\alpha_A) + (r\times\sin\alpha_A)\theta_y - \sigma_x$$
$$+\varepsilon_{zx}(-y_{p1} + \delta_{yx} - (\ell + r\times\cos\alpha_A)\theta_y - \sigma_y)) + \delta_{zx}(1+\varepsilon_{zx}^2)) \quad ----- (16)$$

$$\Delta z'_B = \frac{1}{1+\varepsilon_{zx}^2}(\varepsilon_{xx}((\ell + r\times\sin\alpha_B) - \delta_{yx} + (r\times\sin\alpha_B)\theta_y + (d - r\times\cos\alpha_B$$
$$+(\ell + r\times\sin\alpha_B)\theta_y - \sigma_x)\varepsilon_{zx} + \sigma_y) + \varepsilon_{yx}(d - r\times\cos\alpha_B + (\ell + r\times\sin\alpha_B)\theta_y$$
$$-\sigma_x + \varepsilon_{zx}(-\ell - r\times\sin\alpha_B + \delta_{yx} - (r\times\cos\alpha_B)\theta_y - \sigma_y))$$
$$+\delta_{zx}(1+\varepsilon_{zx}^2)) \quad -----(17)$$

$$\Delta z'_C = \frac{1}{1+\varepsilon_{zx}^2}(\varepsilon_{xx}((-\ell + r\times\sin\alpha_C) - \delta_{yx} + (r\times\sin\alpha_C)\theta_y + (d - r\times\cos\alpha_C$$
$$+(-\ell + r\times\sin\alpha_C)\theta_y - \sigma_x)\varepsilon_{zx} + \sigma_y) + \varepsilon_{yx}(d - r\times\cos\alpha_C + (-\ell + r\times\sin\alpha_C)\theta_y$$
$$-\sigma_x + \varepsilon_{zx}(\ell - r\times\sin\alpha_C + \delta_{yx} - (r\times\cos\alpha_B)\theta_y - \sigma_y))$$
$$+\delta_{zx}(1+\varepsilon_{zx}^2)) \quad -----(18)$$

For the side probe unit, we can obtain the probes' output changes:

$$\Delta y'_D = \frac{1}{1+\varepsilon_{yx}^2}(\varepsilon_{xx}(-(\ell" + r\times\sin\alpha_D) + \delta_{zx} + (r\times\cos\alpha_D)\theta_p + (d - (r\times\cos\alpha_D)$$
$$-(\ell" + r\times\sin\alpha_D)\theta_p - \sigma_x)\varepsilon_{yx} - \sigma_z) + \delta_{yx}(1+\varepsilon_{zx}^2) - (d - (r\times\cos\alpha_D)$$
$$-(\ell" + r\times\sin\alpha_D)\theta_p - \sigma_x + ((\ell" + r\times\sin\alpha_D) - \delta_{zx}$$
$$-(r\times\cos\alpha_D)\theta_p + \sigma_z)\varepsilon_{yx})\varepsilon_{zx}) \quad ----- (19)$$

$$\Delta y'_E = \frac{1}{1+\varepsilon_{yx}^2}(\varepsilon_{xx}(-(\ell" + r\times\sin\alpha_E) + \delta_{zx} + (r\times\cos\alpha_E)\theta_p + (d - (r\times\cos\alpha_E)$$
$$-(\ell" + r\times\sin\alpha_E)\theta_p - \sigma_x)\varepsilon_{yx} - \sigma_z) + \delta_{yx}(1+\varepsilon_{zx}^2) - (d - (r\times\cos\alpha_E)$$
$$-(\ell" + r\times\sin\alpha_E)\theta_p - \sigma_x + ((\ell" + r\times\sin\alpha_E) - \delta_{zx}$$
$$-(r\times\cos\alpha_E)\theta_p + \sigma_z)\varepsilon_{yx})\varepsilon_{zx}) \quad ----- (20)$$

Equations (16 ~ 20) are introduced into Equations (8 ~ 12) and the same process to Simulation I is used to investigate the sensitivity of simplified algorithm when both probe-mounting errors and installment-dependent errors appear simultaneously. In Simulation II(Appendix), the same predefined values of all error motion components to the simulation I are adopted. The results show that the induced errors for rotational error and translational error are at most -1.5×10^{-5} rad ~ 1.5×10^{-5} rad and –0.6 μm ~ 0.6 μm. The ranges are also only about 1/100 of the predefined values. So it can be thought this algorithm is enough robust for the existence of the probe-mounting errors and installment-dependent errors.

7. Conclusion

1. A capacitance-sensor based multi-degree-of-freedom measurement system has been proposed for the miniaturized machine tool to measure five geometric errors simultaneously when one axis moves.

2. Based on homogeneous transformation matrix, the exact mathematical model is derived to establish the relation between the outputs of probes and geometric errors. An algorithm has been developed to calculate individual geometric error component.

3. From the simulation results, the induced errors

could be kept within $1/200$ of the predefined value of every measured geometric error. And during sensitivity analysis this measurement method has better robustness for rotational errors than for translational errors. And the later ones show the increasing trend when the linear displacement become larger.

Further, this proposed system can be constructed and used in error compensation for miniaturized machine tool.

References

1. Subrahmanian, R., Ehman, K., "Development of a meso-scale machine tool (MMT) for micro-machining," Proc. 2002 Japan- USA Symposium on Flexible Automation, Hiroshima, Japan, Vol.1, pp. 163-169, 2002.
2. ASME B5.54, Methods for Performance Evaluation of Computer Numerically Controlled Machining Centers, ASME, 1992.
3. Zhang, C., Ouyang, R., Lu, B., "A displacement method for machine geometry calibration," Annals of the CIRP, Vol. 37, pp. 515-518, 1988.
4. Ni, J., Wu, S., "An on-line measurement technique for machine volumetric error compensation," Journal of Engineering for Industry, Vol. 115, pp. 85-92, 1993.
5. Fan, K., Chen, M., Huang, W., "A six-degree-of-freedom measurement system for the motion accuracy of linear stages," International Journal of Machine Tool & Manufacture, Vol. 38, pp. 155-164, 1998.
6. Paul, R., "Robot manipulators: mathematics, programming, and control, MIT Press, 1981.
7. Weck, M., "Handbook of machine tools, Vol.4: metrological analysis and performance tests, A Wiley-Heyden Publication., 1984.
8. Tu, J., Bossmanns, B., Hung, S., "Modeling and error analysis for assessing spindle radial error motions," Precision Engineering, Vol. 21, pp. 90-101, 1997.
9. Ramesh, R., Mannan, M., Poo, A., "Error compensation in machine tools- a review Part I: geometric, cutting-force induced and fixture-dependent errors," International Journal of Machine Tool & Manufacture, Vol. 40, pp. 1235-1256, 2000.

Appendix

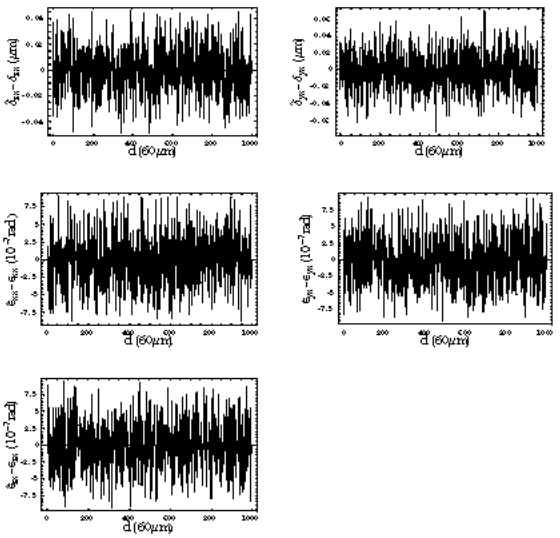

Simulation Parameters:

ε_{xx} , ε_{yx} , ε_{zx} = Random (– 10^{-3} rad, 10^{-3} rad)

δ_{yx} , δ_{zx} = Random (– 50 μm, 50 μm)

ℓ =10000 μm ℓ"=20000 μm d =0~60000 μm

Simulation I Algorithm evaluation results

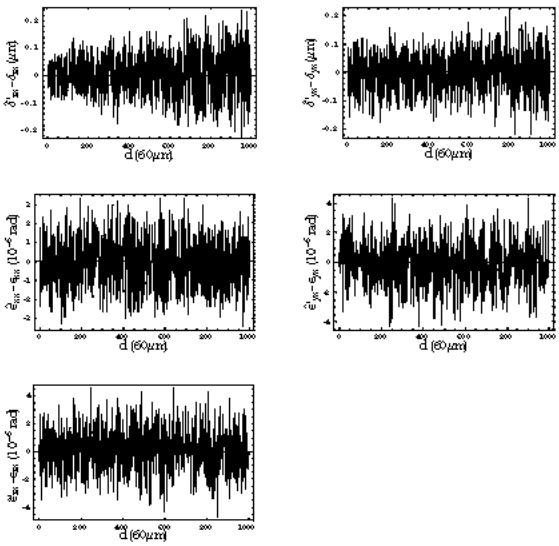

Simulation parameters:

$\theta_y = 0.002; \theta_p = 0.002; \sigma_x = 50\mu m; \sigma_y = 50\mu m$

α_i = random$(0, 2\pi), i = A, B, C, D, E$

(i represents which probe is investigated)

$d = 0 \sim 10000$ μm $r = 10$ μm

Simulation II Sensitivity Analysis Results